JOURNAL OF GEOPHYSICAL RESEARCH, VOL. 105, NO. A12, PAGES 27,685–27,699, DECEMBER 1, 2000

Kelvin-Helmholtz instability on the magnetospheric flanks: An absolute and convective instability approach

Katharine J. Mills, Aaron W. Longbottom, Andrew N. Wright, and Michael S. Ruderman

Mathematical Institute, University of St. Andrews, St. Andrews, Fife, Scotland

Abstract. In this paper, an absolute and convective instability approach to the Kelvin-Helmholtz instability of magnetospheric surface and body/waveguide modes is presented. Rather than considering normal modes individually, the development of localized wavepackets is considered. It is shown that the time asymptotic behavior of such a wavepacket is determined by the double roots of the dispersion relation and that each double root may be identified with a normal mode, for our particular system. The dominant behavior in any reference frame is given by the double root with the largest growth rate. We consider the absolute or convective nature of the instability in the rest frame of the magnetosphere and deduce that in this reference frame wavepackets may only be absolutely unstable (growing at any fixed point in space at large time) close to the nose of the magnetosphere and are convectively unstable (moving away so that at large time there is no disturbance at any fixed point) elsewhere. The e-folding lengths of fast surface mode wavepackets are found to be small but increase around the flanks (these will become nonlinear and lead to the broadening of the low-latitude boundary layer in agreement with previous studies) [*Manuel and Samson*, 1993]. Fast body modes will e-fold only once as they convect around the flanks, so would be expected to remain linear in this region. Slow-mode wavepackets are also studied and are found to have very large e-folding lengths, so that their growth on the flanks will be negligible. The results are compared to a numerical simulation and excellent agreement is obtained.

1. Introduction

It is well known that the Kelvin-Helmholtz instability (KHI) can operate at the magnetopause as suggested by *Dungey* [1954]. Numerous studies of this mechanism have been undertaken, including models of a magnetosphere that extends infinitely away from the magnetopause [e.g., *Sen*, 1964; *Fejer*, 1964; *Southwood*, 1968; *Pu and Kivelson*, 1983]. These studies looked at modes that are exponentially decaying in both the magnetosphere and magnetosheath ("surface" modes) and found that for modes propagating at any particular angle to the flow there exist both lower and upper cutoff speeds corresponding to the onset of instability and the point at which the system restabilizes, respectively. The lower cutoff is zero when the magnetic field is perpendicular to both the flow and the propagation of the modes. The upper cutoff speed becomes very large for modes propagating at large angles to the flow. More recently, studies of a bounded magnetosphere [*Fujita et al.*, 1996; *Mann et al.*, 1999; *Mills et al.*, 1999] have been undertaken. These have studied the unstable behavior of modes that are oscillatory in the magnetosphere ("body" modes) as well as the surface modes. The instability threshold for the body modes is always nonzero, even when the lower cutoff for surface modes is zero. The upper cutoff speed for fast surface modes is removed in this case. *Mills and Wright* [1999] showed that these unstable body modes drive field line resonances (FLRs) in the magnetosphere.

Numerical simulations of the nonlinear behavior of the KHI for the magnetopause surface mode have also been undertaken [e.g., *Miura*, 1984, 1987, 1995a]. These show that the disturbances initially grow at the rate predicted by linear theory and then saturate at later times. The disturbances then form vortices and allow some diffusion of magnetosheath plasma into the magnetosphere, forming a boundary layer just inside the magnetopause (the low-latitude boundary layer (LLBL)). These simulations have, in general, dealt with a periodic domain with a length equal to the wavelength of the initial disturbance. This condition was relaxed by *Miura* [1995a], who found that when two wavelengths of the initial perturbation were included in the box, two small vortices initially formed, which later merged to become one large vortex.

Paper number 1999JA000289.
0148-0227/00/1999JA000289$09.00

In this paper, we study the spatial development of initial disturbances of finite extent (wavepackets rather than normal modes or periodic disturbances) that are driven unstable by the change in shear flow at the magnetopause. In order to do this we use the theory of absolute and convective instabilities (detailed reviews of which may be found in the works of *Briggs* [1964] and *Bers* [1983]). It was first suggested by *Twiss* [1951, 1952] and *Landau and Lifschitz* [1953] that a localized pulse in an unstable system may evolve in two distinct ways, it may be either "convectively" or "absolutely" unstable. The two types of instability are illustrated in Figure 1. An "absolute" instability is one in which the growing pulse expands to encompass all space, so that eventually the disturbance at any fixed point in space grows in time. A "convective" instability is one in which the pulse not only grows, but also propagates away from its starting position so that at any fixed point the disturbance eventually decays in time. The pulse still expands in space but is moving away sufficiently fast that the response of the plasma at large times will be zero at any fixed point. These concepts are frame dependent. If an observer were moving with a growing pulse, he would see a growing disturbance for all time (an absolute instability). Similarly, an observer moving faster than the front edge of a pulse (or slower than the back edge of the pulse) would see a convective instability. Therefore, for any instability we may define a range of reference frames for which the instability is absolute. We can think of the classification of an instability as a measure of the speed with which the fastest growing part of the pulse convects away compared to the rate of broadening of the pulse and the growth rate of the wavepacket.

Studying the absolute or convective nature of an instability gives important insight into the onset of non-

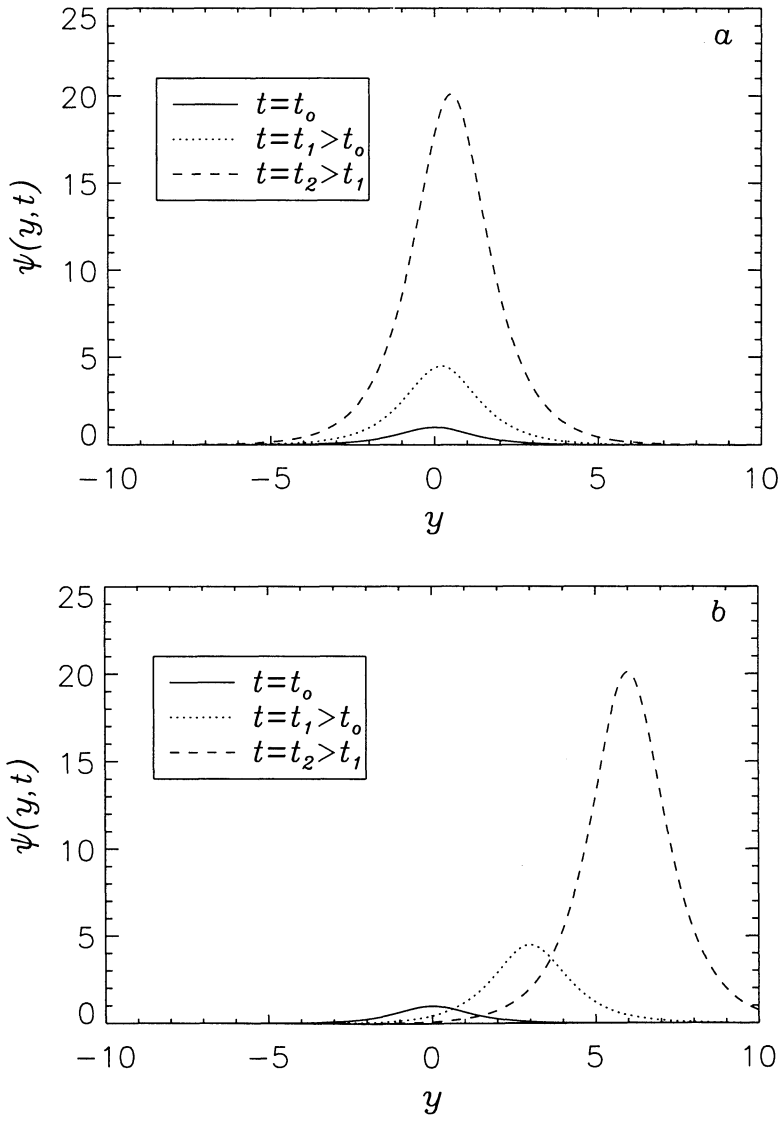

Figure 1. A schematic diagram of the space-time development of (a) an absolute instability and (b) a convective instability.

linear behavior in a system. For example, if an instability is convective and a disturbance will only grow by one factor of e over the length scale of the system then the nonlinear behavior is unlikely to be important. Conversely, if the pulse is found to be dominated by a surface wave that will grow to a significant amplitude within the system, then in analyzing the nonlinear behavior we may choose to simplify the equations and consider only surface modes.

Wu [1986] states that the KHI at the magnetopause should be convectively unstable. However, Wu uses the term convective instability in a rather informal fashion compared to our definition above and the body of literature that this paper draws on, limiting the definition to implying that disturbances should propagate tailward with a finite velocity. Wu took a numerical box much larger than the initial perturbation with a symmetric flow profile and found that the disturbance expanded to fill the box. The symmetry in Wu's model meant that his simulation frame was actually moving with the fastest growing part of the disturbance so that the pulse remained centered on the simulation domain. Therefore in this reference frame the instability is absolute. However, showing that an instability is absolute in one reference frame tells us nothing about its behavior in other frames. Wu's calculation did not take into account the effect of changing the reference frame, so he is unable to state whether the instability is absolute or convective in the rest frame of the magnetosphere.

Manuel and Samson [1993] investigated the spatial development of the KHI along the magnetopause using an MHD simulation in which seed perturbations were fed in at the upstream end and an outgoing boundary condition was applied at the downstream end of the waveguide. Their simulation showed the classic behavior of a convective instability, although they did not use this term (the disturbances convected downstream as they grew, only showing nonlinear behavior several Earth radii (R_E) from their source).

Miura [1995b] summarizes the results from numerical simulations of the KHI at the magnetopause and presents a picture of an undulating magnetopause cause by vortices travelling tailward along the flanks. This is a qualitative description of a convective instability around the magnetospheric flanks, although Miura does not use that phrase.

The concepts of absolute and convective instabilities have been applied to the magnetosphere in the work of *Wright et al.* [2000]. Here we present a fuller treatment of the modes in that model and compare our results to those from a numerical simulation. Some of the content of this paper is rather technical, and some readers may find the distinction between convective and absolute instabilities based on physical behavior (mentioned earlier) more appealing. This description has been expounded more fully by *Wright et al.* [2000] to which we direct interested readers (particularly section 2 and the discussion of Figure 1 in that paper).

In section 2 of this paper we describe the mathematical method for distinguishing between absolute and convective instabilities (more details of which may be found in the appendix), and in section 3 we outline our model and the governing equations. We detail our results in section 4 and compare these to results from a numerical simulation in section 5. Finally, in Section 6 we discuss the implications of our results for the magnetosphere.

2. Absolute and Convective Instabilities

Previous studies of the KHI at the magnetopause have considered normal modes of the system. However, in order to determine the absolute or convective nature of the instability we must instead consider a wavepacket. In fact, this is more realistic as it is unlikely that the entire magnetopause will be excited monochromatically at any time. The wavepacket may then be expressed as a Fourier integral over the normal modes of the system. It turns out that determining the space-time evolution of such a wavepacket is more complicated than simply determining whether any of the normal modes may be unstable.

The space-time evolution of a wavepacket in an unstable system is determined by finding all the double roots or the dispersion relation for that system ($D(\omega, k_y) = 0$), such that

$$D(\omega, k_y) = \frac{\partial D}{\partial k_y}(\omega, k_y) = 0. \tag{1}$$

The behavior of the disturbance, $\psi(y,t)$ is then given by the double root that has the largest imaginary part of ω, ω_s say (corresponding to a complex value of k_y, k_s say). Then, as $t \to \infty$,

$$\psi(y,t) \sim \frac{1}{\sqrt{t}} \mathrm{e}^{-i\omega_s t} \mathrm{e}^{ik_s y}, \tag{2}$$

where ψ represents the response of the plasma as a function of y and t. (See *Wright et al.* [2000], *Bers* [1983], or *Briggs* [1964] for more details.) If ω_s has a positive imaginary part, (2) indicates that

$$\psi(y,t) \to \infty \qquad t \to \infty, \tag{3}$$

in other words, the instability is absolute. Conversely, if the imaginary part of ω_s is negative, we find that

$$\psi(y,t) \to 0 \qquad t \to \infty, \tag{4}$$

indicating that the instability is convective. These asymptotic formulae are valid for any fixed point in the reference frame in which we have defined $D(\omega, k_y)$. If we change reference frame we find that both the frequency and wavenumber of any double root are changed, and so the time asymptotic behavior of the pulse is different in different reference frames. Thus, by tracing the double roots in different reference frames (moving

with speeds denoted by v_f) we may determine the nature of the instability in all of those reference frames. For clarity, we will denote by γ the value of the growth rate at a double root in order to distinguish it from ω_i, the growth rate of a normal mode.

For convective instabilities an important quantity in determining the effects of a wavepacket on the magnetosphere is its spatial growth rate. It may be shown that the maximum spatial growth rate of the wavepacket (when viewed from the magnetospheric rest frame) is $\gamma(v_{f1})/v_{f1}$, where v_{f1} satisfies [see *Brevdo*, 1994]

$$\frac{d\gamma(v_f)}{dv_f} = \frac{\gamma(v_f)}{v_f}. \tag{5}$$

Graphically, this corresponds to the line from the origin to a point on the curve $\gamma(v_f)$ being a tangent to the curve at that point [see *Wright et al.*, 2000]. A more thorough discussion of the results quoted in this section may be found in Appendix A. Detailed reviews of the theory of absolute and convective instabilities may be found in the works of *Briggs* [1964] and *Bers* [1983].

3. Model and Governing Equations

In order to model the space-time evolution of both body and surface modes in the magnetosphere, we have modeled a uniform, bounded static magnetosphere separated from a uniform, semi-infinite flowing magnetosheath by a boundary layer of finite width over which the equilibrium flow speed changes continuously (this boundary layer serves to limit the growth rate of modes, see *Walker* [1981]). A sketch of this model is shown in Figure 2. Throughout this paper we use variables normalized to the equilibrium sound speed c_{s2} and density ρ_{o2} in the magnetosheath and the width of the magnetospheric cavity (from the inner boundary to the middle of the boundary layer), d. (Time is normalized by the quantity d/c_s, pressure by ΓP_2, and magnetic fields by $\sqrt{\Gamma P_2 \mu_o}$, where P_2 is the equilibrium pressure in the magnetosheath and Γ is the ratio of specific heats which we take to be 5/3.) The boundary layer is thus centered at $x = 1$ and has width 2δ. We are modeling the equilibrium on the equatorial flanks of the magnetosphere so the equilibrium magnetic field in the magnetosphere, $\mathbf{B_1}$ is perpendicular to the equilibrium flow in the magnetosheath, $\mathbf{v_o}$. In order to consider both fast and slow modes we have taken a finite plasma beta β in the magnetosphere, so that we have an equilibrium plasma pressure P_1 with an equilibrium density ρ_{o1}. In both the magnetosphere and the magnetosheath the plasma parameters are taken to be constant and variation only occurs within the boundary layer, $1 - \delta < x < 1 + \delta$. In this region the flow speed profile is taken to be

$$v(x) = \frac{v_o}{2} + \frac{v_o}{4}\left\{\frac{3(x-1)}{\delta} - \frac{(x-1)^3}{\delta^3}\right\}. \tag{6}$$

This cubic form of the velocity profile was suggested by *Walker* [1981] and allows both the flow velocity and its first derivative to be continuous at the edges of the boundary layer, $x = 1 \pm \delta$. The other equilibrium parameters of the plasma (magnetic field, plasma pressure, etc.) are assumed to change discontinuously from the magnetospheric values to those in the magnetosheath at the inner edge of the boundary layer ($x = 1 - \delta$). Thus, in the boundary layer, there is no magnetic field and only a plasma pressure P_2. This eliminates the possibility of having Alfvén resonances within the boundary layer which simplifies the physics that we are considering. The jump in flow speed across the boundary is denoted by $\Delta v = v(1+\delta) - v(1-\delta)$, which is a frame-independent variable.

Our principal motivation for introducing a boundary layer is that it removes the unbounded growth rates that occur for a discontinuity in equilibrium flow, which would make our initial value/wavepacket formulation ill posed. The existence of a boundary layer is also supported by observations, although these show that

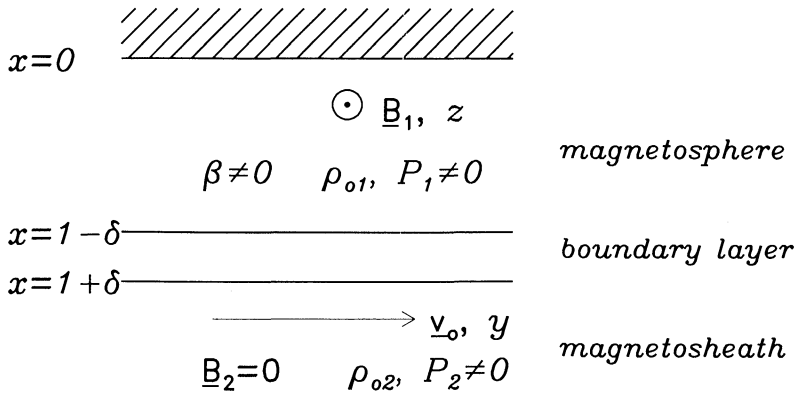

Figure 2. A schematic diagram of our bounded magnetosphere model containing a finite width boundary layer.

there can be a significant magnetic field in the boundary layer and the magnetosheath. The presence of such a field adds a degree of complexity that we do not wish to consider in this preliminary study: It is well known that the sheath field can have a stabilizing effect. It is less well known that a field in the boundary layer can give rise to slow and Alfven resonances that (through the action of negative energy waves) can make the system more unstable [e.g., *Ruderman and Wright*, 1998]. The influence of both these effects on the evolution of wavepackets deserves further attention but is beyond the scope of the present paper.

We may derive analytic solutions of the linearized MHD equations in the magnetosphere and magnetosheath since these regions are uniform. In doing this we consider perturbations proportional to $e^{i(k_y y + k_z z - \omega t)}$, where ω is the frequency of the oscillations in the magnetospheric rest frame (which may, in general be complex, $\omega = \omega_r + i\omega_i$) and k_y and k_z are the components of the wavenumber in the y and z directions, respectively. We have taken the boundary at $x = 0$ to be perfectly reflecting and set the x component of the perturbed velocity to zero there. In the magnetosheath we require the x component of the group velocity to be directed away from the magnetopause boundary in the reference frame moving with the flowing plasma. This requirement leads to the condition that [see also *Mann et al.*, 1999; *Mills et al.*, 1999]

$$\mathrm{Re}\,(\omega_o')\,\mathrm{Re}\,(m_2) + \mathrm{Im}\,(\omega_o')\,\mathrm{Im}\,(m_2) > 0, \qquad (7)$$

where ω_o' is the Doppler-shifted frequency is given by $\omega_o' = \omega - kv_o \sin\alpha$ in the rest frame of the magnetosheath, and m_2 is the component of the complex wavenumber in the magnetosheath in the x direction defined as

$$m_2^2 = \frac{\omega_o'^2 - k^2 c_{s2}^2}{c_{s2}^2}. \qquad (8)$$

Here we have used the definitions $k = \sqrt{k_y^2 + k_z^2}$ and $\alpha = \tan^{-1}(k_y/k_z)$. These conditions allow us to determine the solutions of the equations in the magnetosphere and magnetosheath to within an arbitrary phase and amplitude.

In the boundary layer we may combine the linearized hydrodynamic equations (since there is no magnetic field in this region) to obtain two first-order ordinary differential equations for the pressure perturbation, p_T (which is the same as the plasma pressure perturbation in this region since the magnetic field is zero), and the displacement in the x direction ($= u_{x1}/[\omega - kv(x)\sin\alpha]$, where u_{x1} is the component of the perturbed velocity in the x direction). The two equations are

$$\frac{dp_T}{dx} = i\rho_{o2}\omega'^2(x)\left(\frac{u_{x1}}{\omega'(x)}\right) \qquad (9)$$

$$\frac{d}{dx}\left(\frac{u_{x1}}{\omega'(x)}\right) = \frac{im^2(x)}{\rho_{o2}\omega'^2(x)} p_T,$$

where $m^2(x)$ is the x component of the complex wavenumber in the boundary layer, defined by

$$m^2(x) = \frac{\omega'^2(x) - k^2 c_{s2}^2}{c_{s2}^2}, \qquad (10)$$

and $\omega'(x) = \omega - kv(x)\sin\alpha$ is the Doppler-shifted frequency at x.

Taking the phase of the solution in the magnetosphere to be zero and its amplitude to be one, we use the analytical solutions in the magnetosphere to find the values of the perturbed total pressure and x component of displacement ($\xi_x = u_{x1}/\omega'$) at $x = 1 - \delta$ since the total pressure and x displacement are continuous everywhere. We then use a fourth order Runge-Kutta scheme to integrate across the boundary layer and match the solutions at $x = 1 + \delta$ to those from the solution in the magnetosheath to find the eigenvalues of our problem.

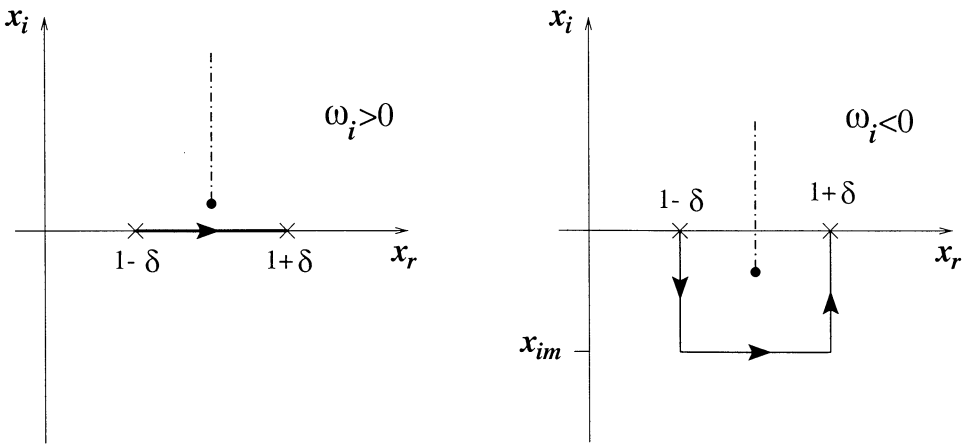

Figure 3. The integration contours in the complex x plane for (left) $\omega_i > 0$ and (right) $\omega_i < 0$. The dotted-dashed line indicates the position of the branch cut.

However, for real ω, there is singularity and branch cut associated with (9) where

$$\omega'(x) = \omega - kv(x)\sin\alpha = 0, \tag{11}$$

which inhibits integration along the real x axis. In order to overcome this we may instead integrate in the complex x plane around the singularity. In this case we find that the position at which the singularity occurs has a positive imaginary part of x when $\omega_i > 0$ (see Figure 3). Therefore we must ensure that we always integrate beneath the singularity (i.e., we are taking the branch cut associated with the singularity to be directed upward in the complex x plane). For simplicity, we place our integration contour so that we first integrate from $x = 1 - \delta$ to $x = 1 - \delta + ix_{im}$ (where $x_{im} \leq 0$), and then to $x = 1 + \delta + ix_{im}$, and finally to $x = 1 + \delta$ (see Figure 3). In general, when we consider unstable modes, we may take $x_{im} = 0$, but when the growth rate is small we find that it is easier to take a nonzero value of x_{im} since the integration needs a very fine grid to converge if the singularity is too close to the real x axis. When $\omega_i \leq 0$, we must take $x_{im} < 0$. If x_{im} is not sufficiently large, the branch cut will not be circumvented. This will result in the integration path arriving at $x = 1 + \delta$ on a different Riemann sheet to that required for a physical solution. This behavior manifests itself as poor numerical convergence as the singularity nears the integration contour, and a jump in the solution at $x = 1 + \delta$ as it crosses the contour, corresponding to the switching from one Riemann sheet to another.

We have taken a maximum step size of $\sim 5 \times 10^{-4}$ in our Runge-Kutta scheme, giving a maximum global error of $\sim 10^{-10}$. In our Newton-Raphson root finder we have found the roots to within $\nu \leq 10^{-6}$.

4. Results

4.1. Double Roots Corresponding to Fast Surface Modes

In this section we investigate the behavior of double roots that are associated with fast surface modes. In order to find the double roots we must first solve the dispersion relation to identify the maxima of the growth rate. Figure 4 shows the effect of a finite width boundary layer on the phase speed ($v_{ph} = \omega_r/k$) and growth rate, ω_i, of the fast surface mode when $v_o = 2$ and for modes propagating parallel to the flow in the magnetosphere (so that $\alpha = \pi/2$). We have taken $\delta = 0, 0.05, 0.1$ shown by the solid, dashed, and dotted-dashed lines, respectively. Increasing the value of δ decreases both the phase speed and growth rate from their values for an infinitely thin magnetopause. Indeed, in the $\delta = 0$ case the growth rate is unbounded for large k, but when $\delta \neq 0$ the growth rate has a maximum for finite k and decays toward zero as k continues to increase. This is in agreement with the result found by *Walker* [1981].

Figure 5 shows the asymptotic growth rate γ as a function of reference frame speed v_f for the fast surface mode wavepacket when $\Delta v = 2$ and $\alpha = \pi/2$ for different values of δ. These curves indicate that this mode is associated with a convective instability when $v_f = 0$ (i.e., in the rest frame of the magnetosphere) since $\gamma < 0$. The values of v_f at which $\gamma(v_f) = 0$ will correspond to the speed at which the front and back of the growing wavepacket will move in the magnetospheric rest frame with constant amplitude. In frames with $v_f < 0.15$ the wavepacket will run ahead of the observer leaving no disturbance for large time. Conversely, frames with $v_f > 1.73$ correspond to the observer running ahead of the wavepacket and, again, seeing no dis-

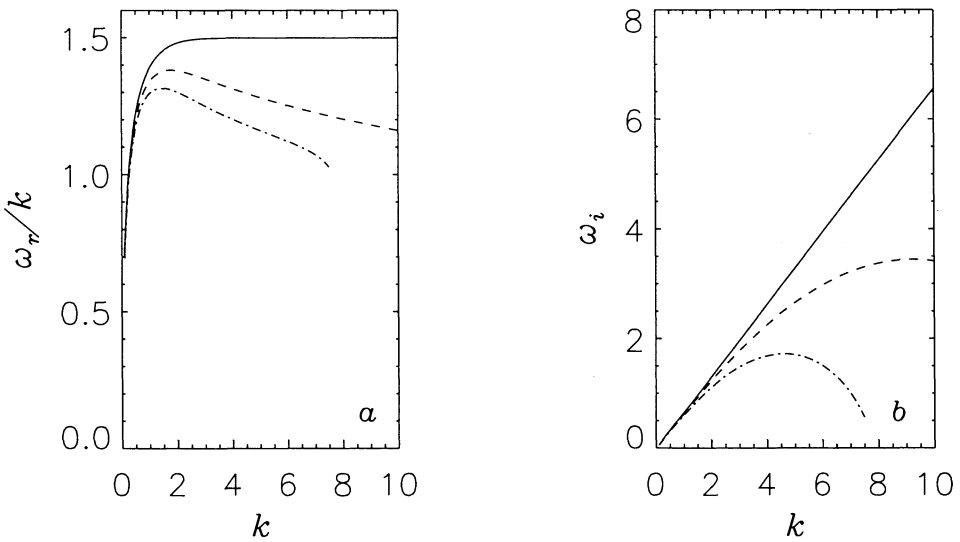

Figure 4. The (a) phase speeds and (b) growth rates of the fast surface mode when $v_o = 2$ and $\alpha = \pi/2$ for $\delta = 0$ (solid line), $\delta = 0.05$ (dashed line), and $\delta = 0.1$ (dotted-dashed line).

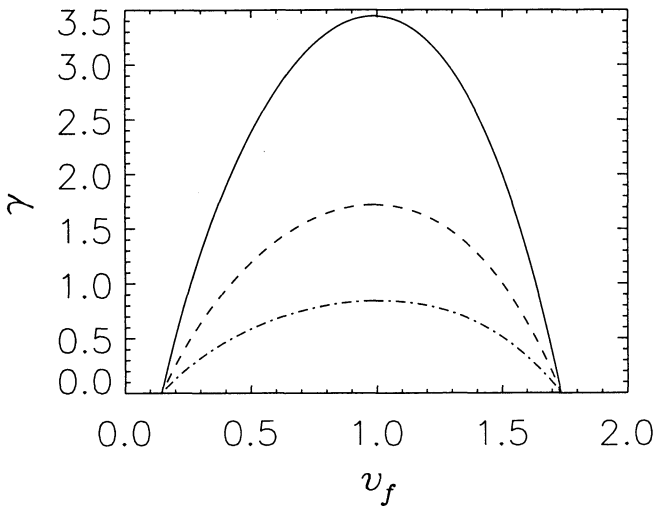

Figure 5. The growth rate γ of the fast surface mode wavepacket as a function of reference frame v_f for $\Delta v = 2$ when $\delta = 0.05$ (solid line), $\delta = 0.1$ (dashed line), and $\delta = 0.2$ (dotted-dashed line).

turbance for large time. The maximum gamma occurs at for the value of v_f corresponding to the group velocity of the wavepacket, i.e., the maximum growth rate is seen by an observer who moves so as to just keep up with the wavepacket. The maximum value of γ scales as $1/\delta$, and the range of reference frames for which the instability is absolute ($\gamma > 0$) is identical for all nonzero δ. Physically, this corresponds to the surface mode being confined to the vicinity of the boundary layer and being insensitive to the inner boundary where the amplitude is very small. The spatial growth rate of these modes will also scale as $\sim 1/\delta$, so that the e-folding length will be proportional to δ.

Next we look at the dependence of the function $\gamma(v_f)$ on the change in plasma flow speed Δv. Figure 6 shows the asymptotic growth rate, $\gamma(v_f)$, when $\delta = 0.1$ and $\alpha = \pi/2$ for various values of Δv. The mode indicates a convective instability in the rest frame of the magnetosphere for all flow speeds except $\Delta v = 0.5$ (shown here by a dotted-dashed line), which would only occur near to the nose of the magnetosphere. Thus, for most of the flanks of the magnetosphere the fast surface mode wavepacket corresponds to a convective instability. For a given value of δ we can see that the maximum growth rate initially grows as the flow speed increases from zero but then decreases as Δv increases from ~ 1. The spatial growth rate will be largest for small flow speeds and decreases as the flow speed increases. Determining the range of frame speeds (v_f) for which γ is positive or negative is crucial in determining the nature of the instability in a given frame, such as the magnetospheric rest frame. It is evident from our results that the nature of the instability in a given frame is dependent on the value of Δv, among other things. Although the trends are clear from our diagrams, we have not identified any simple relations for identifying the different v_f regimes.

We have also considered fast surface modes propagating nonparallel to the magnetosheath flow (not shown here). We found that the asymptotic growth rate is always largest for modes propagating parallel to the flow and the maxima of the asymptotic growth rate occurs for lowest v_f when the modes propagate parallel to the flow.

4.2. Double Roots Corresponding to Fast Body Modes

The bounded nature of the magnetosphere in the model we have considered allows the propagation of modes that are oscillatory in the magnetosphere (body modes) as well as surface modes. In this section we consider the behavior of double roots corresponding to fast body modes. Figure 7 shows the effect of a nonzero width boundary layer on the dispersion of these modes. Like the fast surface mode, the growth rate is generally reduced and the maximum occurs for lower k as δ is increased. The phase speed is generally reduced as well but not as significantly as in the case of the surface mode. The effect on the growth rate is greater for the second harmonic (Figure 7d) than for the first (Figure 7b).

Figure 8 shows the asymptotic growth rate γ as a function of v_f for the fundamental fast body mode when $\delta = 0.1$ and $\alpha = \pi/2$. We have taken $\Delta v = 5, 7.5$, and 10, shown here by the solid, dashed, and dotted-dashed lines, respectively. For all these values of the flow speed we find that the double root indicates a convective instability in the rest frame of the magnetosphere, and the lower value of v_f for which $\gamma = 0$ is very similar for all the curves. As the flow speed increases, the maxi-

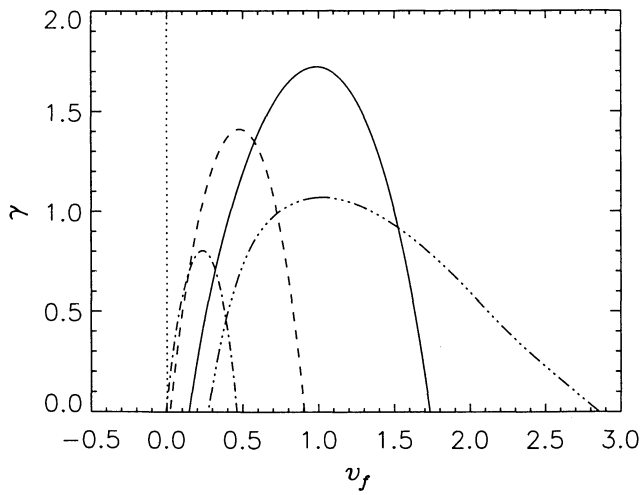

Figure 6. The growth rate γ of the fast surface mode wavepacket as a function of reference frame v_f for $\Delta v = 0.5$ (dotted-dashed line), $\Delta v = 1$ (dashed line), $\Delta v = 2$ (solid line), and $\Delta v = 5$ (triple-dotted-dashed line).

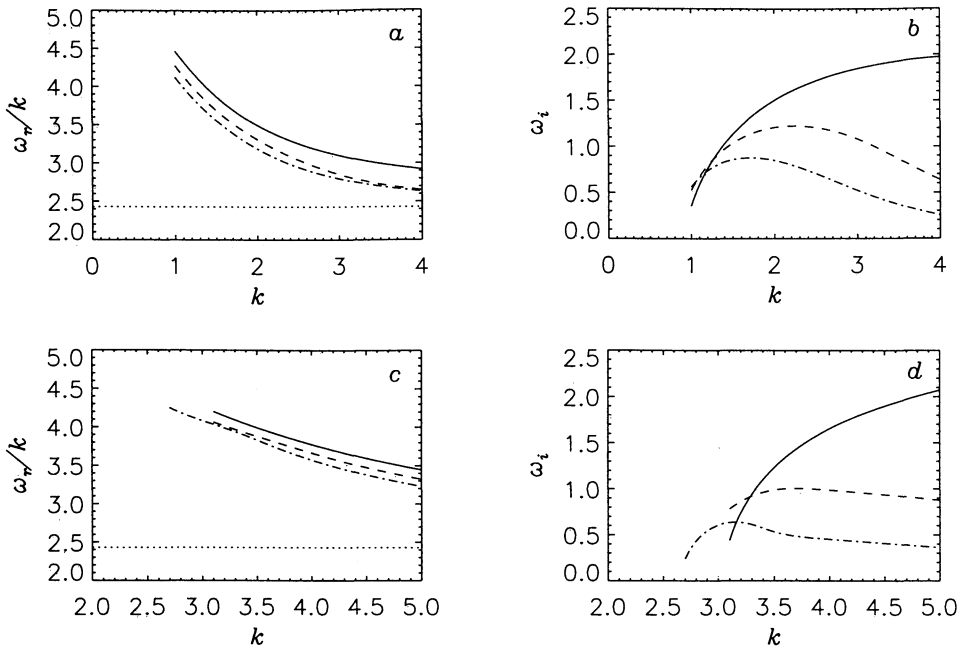

Figure 7. (a,b) Fundamental mode and (c,d) second harmonic. The (left) phase speeds and (right) growth rates of the fast body mode harmonics when $v_o = 5$ and $\alpha = \pi/2$ for $\delta = 0$ (solid line), $\delta = 0.05$ (dashed line), and $\delta = 0.1$ (dotted-dashed line). The dotted lines in Figures 7a and 7c show the value of the fast speed c_f in the magnetosphere.

mum value of the growth rate increases, and the range of reference frames for which the instability is absolute also increases.

Next we consider the effect of a nonzero k_z on the double roots of this mode. Figure 9 shows $\gamma\,(v_f)$ for the fundamental fast body mode when $\Delta v = 5$ and $\delta = 0.1$ for different values of α. As we decrease α from $\pi/2$, we see that the maximum growth rate decreases slightly and occurs for higher v_f. These double roots still indicate a convective instability in the rest frame of the magnetosphere.

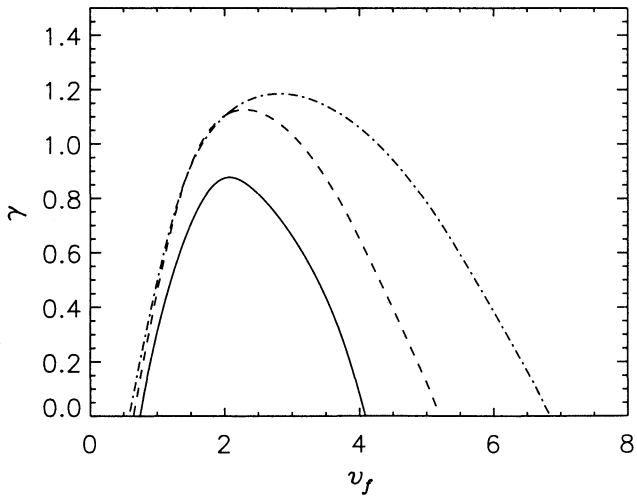

Figure 8. The growth rate γ of the fundamental fast body mode wavepacket as a function of reference frame v_f for $\Delta v = 5$ (solid line), $\Delta v = 7.5$ (dashed line), and $\Delta v = 10$ (dotted-dashed line) when $\alpha = \pi/2$.

5. Results From a Numerical Simulation

In order to help interpret our results we have compared them to the results from a two-dimensional $(x-y)$ time-dependent code that solves the linear MHD equations for the equilibria described in the previous sections. The code uses a staggered mesh on which the equilibrium variables together with their derivatives are defined. The perturbed velocity and total pressure are advanced in time using Hymans third-order predictor-corrector method with fourth-order differencing in space. The computational domain lies between $x = [0 : 10]$ and $y = [-60 : 60]$. The boundary conditions are periodic in the y direction, and no normal velocity (with the appropriate symmetry conditions for the other variables) is imposed in the x direction. For the cases illustrated here the spatial grid sizes for the numerical integration (dx and dy) are taken to be 0.025, and energy is conserved to within $1000th$ of a percent. Note that although our simulation is periodic in y, we have taken the boundaries to be so far away that negligible wave energy reaches them.

Our boundary conditions at $x = 0$ and 10 provide perfect reflection. This is desirable at $x = 0$, as the Alfven speed variation in the real magnetosphere refracts waves, which is mimiced by simple reflection in our model. The boundary condition at $x = 10$ has little

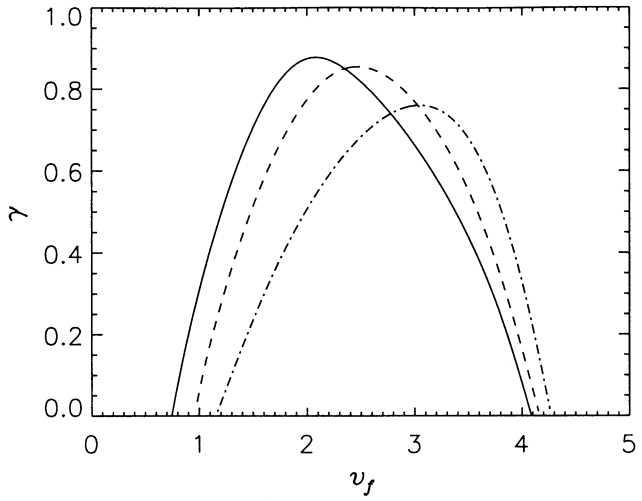

Figure 9. The growth rate γ of the fundamental fast body mode wavepacket as a function of reference frame v_f for $\Delta v = 5$ when $\alpha = \pi/2$ (solid line), $\alpha = \pi/3$ (dashed line), and $\alpha = \pi/4$ (dotted-dashed line) and $\delta = 0.1$.

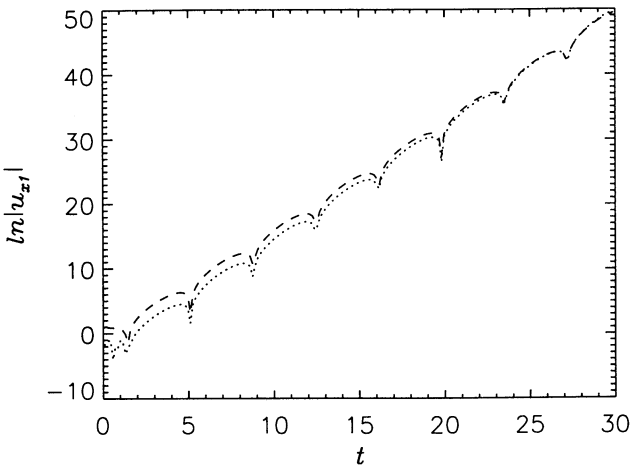

Figure 11. The logarithm of the absolute value of the perturbed velocity found by the numerical simulation (dotted line) and that predicted by our asymptotic analysis (dashed line) at $x = 0.5$ and $y' = 0$ in the reference frame $v_f = 1$ and with $\Delta v = 2$.

effect on the solution since the amplitude of the unstable wavepackets decreases exponentially with x and so is small there. Indeed, this was verified in other runs where the boundary was moved in x and no difference in the behavior of the solution was observed.

In this simulation we perturb the equilibrium and allow the system to evolve in time. The initial perturbation is taken to have a wavelength in the y direction similar to that of the fastest growing normal mode and is contained within an envelope, so that overall, the y dependence of our initial displacement is given by

$$u_{x1}(y) = \frac{1}{2}\left[1 + \cos\left(\frac{2\pi y}{5}\right)\right]\cos(k_y y)\,; -2.5 < y < 2.5, \tag{12}$$

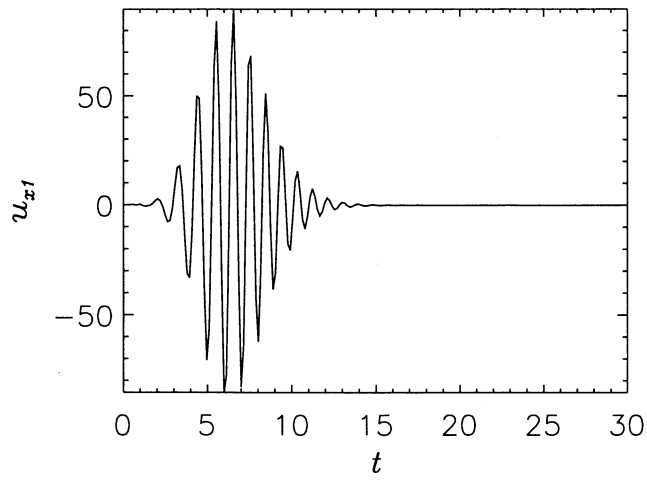

Figure 10. The perturbed velocity in the x direction as a function of t for $y = 2.5$ in the rest frame of the magnetosphere ($v_f = 0$) at $x = 0.5$ and with $\Delta v = 2$.

and $u_{x1} = 0$ elsewhere. The x dependence of the perturbation is chosen to be surface mode like in the first case (when $\Delta v = 2$) as it is only surface modes that will be excited. In the $\Delta v = 5$ case, body modes will also be excited, and we have used a quarter wavelength variation in x within the magnetosphere for the initial perturbation.

First, we examine the case where $\Delta v = 2$ and $\alpha = \pi/2$, when the only unstable normal mode is the fast surface mode. We have taken $\delta = 0.1$ and the asymptotic growth rate as a function of v_f in this case is shown by the dashed line in Figure 5. Figure 10 shows the x component of the perturbed velocity as a function of time in the rest frame of the magnetosphere at $y = 2.5$ (the leading edge of the pulse) and $x = 0.5$. The perturbation passes over the observer and the signal at large times is zero. This confirms that the instability is convective in the rest frame of the magnetosphere.

Now we consider the evolution of the disturbance in a reference frame moving with $v_f = 1$. Here we expect to find an absolute instability since $\gamma(1) > 0$ (see Figure 5). In Figure 11 we have plotted the disturbance at the point $y' = 0$ (where $y' = y - v_f t$) as a dotted line, and we have overplotted the evolution that our asymptotic analysis (Equation (2) predicts as a dashed line. We have matched the phase and amplitude of the results at $t = 30$. The agreement between the prediction and the numerical results is excellent. In this case the growth rate predicted by our analysis is 1.72, and the global growth rate of the system in the numerical simulation (which should be close to that of the fastest growing mode) is 1.74.

In Figure 12 we have plotted the position of the pulse in y at lots of different times to get an idea of the spatial growth rate of the mode. We have taken a reference frame moving with $v_f = -29$ in which we would expect

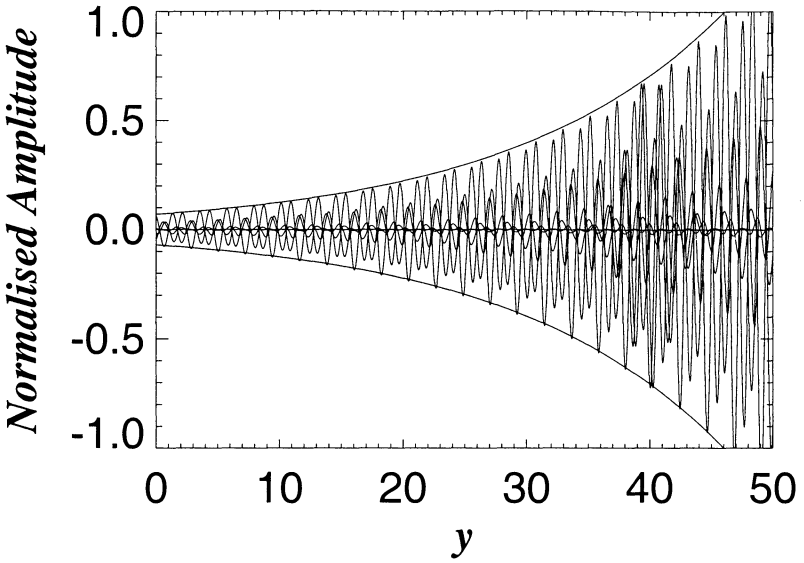

Figure 12. The position of the wavepacket in y at various times plotted one over the other. The solid lines give the envelope of spatial growth predicted by our asymptotic analysis.

the instability to be convective. We have chosen this reference frame so as be able to clearly see that spatial growth of the disturbance as it propagates along. The solid line indicates the envelope predicted by our spatial growth rate calculation and fits the numerical data very well.

Next we compare our predictions and numerical simulations for the case when $\Delta v = 5$, $\alpha = \pi/2$, and $\delta = 0.1$. Figure 13 shows the value of γ at the double roots corresponding to the fast surface mode (dot-dashed line) and the first and second harmonics of the fast body mode (solid and dashed lines, respectively). We expect the system to be convectively unstable in the rest frame of the magnetosphere, and in reference frames moving with speeds $0.3 \lesssim v_f \lesssim 1.5$ we expect the dominant plasma response to be that of a surface mode. The fundamental fast body mode will dominate in reference frames in the range $1.5 \lesssim v_f \lesssim 3.2$. The peak in γ of the double root corresponding to the second fast body mode harmonic occurs below the curve of the fundamental mode since the group velocities at maximum growth rate of the two modes are similar. The second harmonic will dominate for $3.3 \lesssim v_f \lesssim 4.3$.

Figure 14 shows the disturbance as a function of y' (in the reference frame $v_f = 1.8$) when $t = 20$ and at

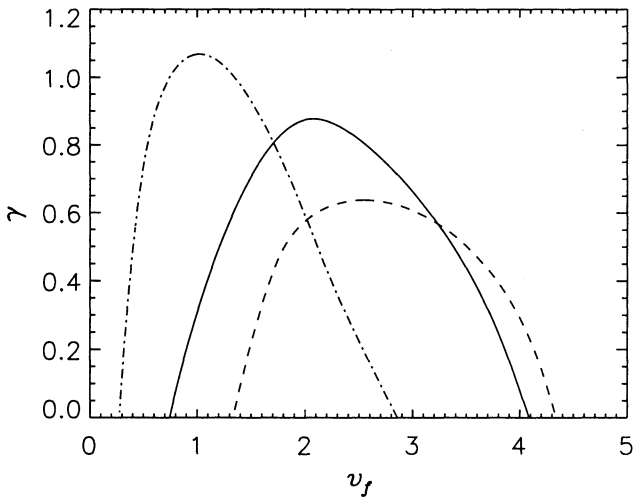

Figure 13. The growth rates γ of the fast mode wavepackets as a function of reference frame v_f for $\Delta v = 5$ when $\alpha = \pi/2$ and $\delta = 0.1$. The roots shown may be identified with the fundamental body mode (solid line), the second harmonic (dashed line), and the surface mode (dotted-dashed line).

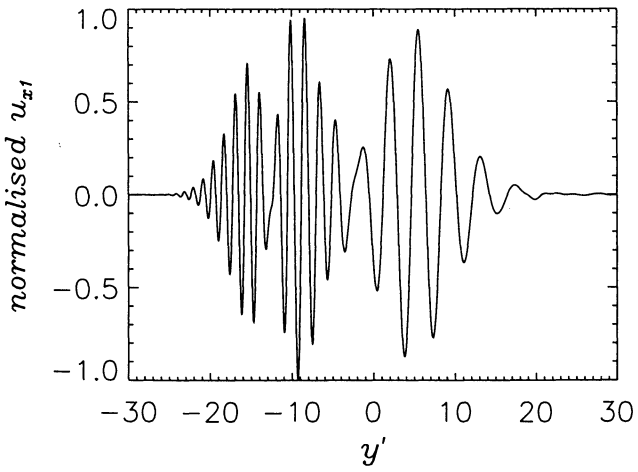

Figure 14. The perturbed velocity in the x direction as a function of y' when $t = 20$ at $x = 0.5$ and in the reference frame moving with $v_f = 1.8$.

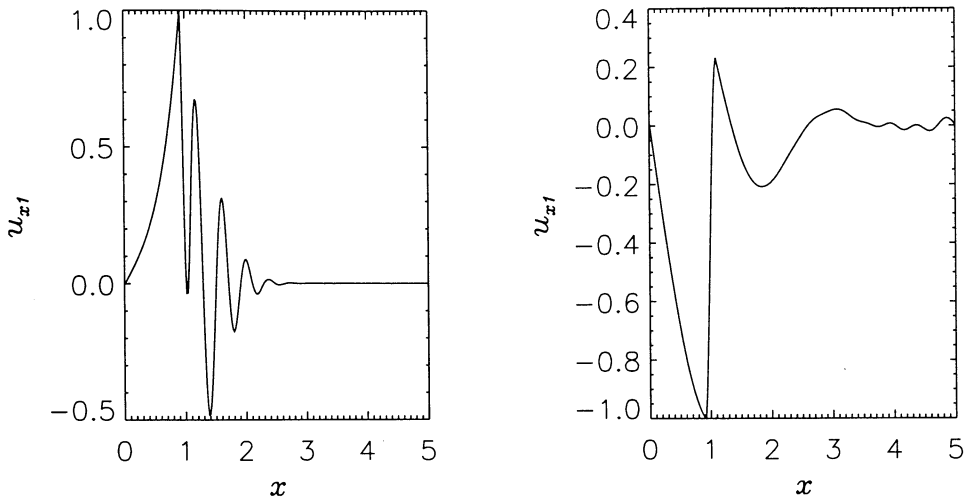

Figure 15. The perturbed velocity in the x direction as a function of x when $t = 20$ in the frame moving with $v_f = 1.8$ at (left) $y' = -15$ and (right) $y' = 7.5$ (see Figure 14).

$x = 0.5$. We can clearly see that the initial pulse has largely split into two separate shapes, one moving slower than this reference frame and one moving faster. Looking at Figure 13, we expect the fast surface mode part of the pulse to move at a speed of -0.8 in this reference frame, which at $t = 20$ would correspond to a position of $y' = -16$. There is indeed a pulse centered at that point. Similarly, we would expect the center of the fast body mode pulse to have moved to position of $y' = 6$, which again agrees well with Figure 14. The pulse centered around $y' = -9$ is formed because of the interference of the front of the fast surface mode disturbance with the tail end of the body mode disturbance. We can also use this plot to estimate the wavelengths, λ at the centers of the wavepackets and compare them to our predictions. For the fast surface mode we predict a wavelength of $\lambda = 1.3$ and the simulation gives $\lambda = 1.4$. For the fast body mode we predict $\lambda = 3.7$, and the simulation also gives this value. Once again, the agreement between our predictions and the numerical simulation are excellent. Figure 15 shows the cross sections in x of these two parts of the pulse. The first plot shows a cut along $y' = -15$ in Figure 14. The perturbation has a classic "surface mode" character in the magnetosphere and has a decaying oscillation into the magnetosheath. The second plot shows a cut along $y' = 7.5$ in Figure 14, and the perturbation is a body mode with a quarter of a wavelength trapped in the magnetosphere. This agrees well with our predictions of the evolution of the two types of mode.

Our prediction for the asymptotic growth rate in the reference frame moving with $v_f = 1.8$ for this case gives $\gamma = 0.84$ and a frequency of 2.72. Thus, in this frame we have an absolute instability and from Figure 13 we see that the fundamental waveguide mode wavepacket will dominate at large t. The fast surface mode wavepacket is also absolutely unstable in this reference frame, but it has a smaller growth rate. The results from the numerical simulation give the frequency as 2.7 and the growth rate as 0.84, so the agreement is again excellent.

6. Discussions and Conclusions

We have shown that (except for the fast surface mode when the magnetosheath flow speed is very small) the double roots corresponding to both fast body and surface modes indicate that the magnetopause is convectively unstable to the KHI in the magnetospheric rest frame. Thus the most important factor in determining the effect on the equilibrium of these unstable disturbances is their spatial growth rate (or their e-folding length).

We have shown that the system is only absolutely unstable when the flow speed is very small, which corresponds to the nose of the magnetosphere, where the boundary layer is very thin and the validity of MHD is questionable. Elsewhere, the system is convectively unstable. The e-folding length of the fast surface mode (when convectively unstable) ranges from $\sim 1\ R_E$ for low values of flow speed ($\Delta v = 2$) and $\delta = 0.01$ (close to where we expect the modes to begin being excited) to $\sim 7\ R_E$ when $\Delta v = 5$ and $\delta = 0.1$ (corresponding to the equilibrium further around the magnetospheric flanks). From these values we see that the surface mode disturbances will initially grow very quickly as they convect around the magnetosphere, so that nonlinear effects will dominate. This is in agreement with *Manuel and Samson* [1993], who showed that the nonlinear effects can broaden the boundary layer. Further around the flanks the spatial growth rate reduces and the disturbances will not grow very much larger before reaching the magnetotail, which is expected to be more stable. (We assume that the total distance from the nose around the flanks to the start of the magnetotail to be $\sim 30\ R_E$).

The fast body modes may only become unstable when

$$\Delta v > \frac{c_f + c_{s2}}{\sin \alpha}, \tag{13}$$

where c_f is the fast speed in the magnetosphere [see *Mills et al.*, 1999]. Therefore they may only become unstable away from the nose of the magnetosphere. In this region we find e-folding lengths of the order of 20 R_E, indicating that these modes will not grow significantly as they convect around the magnetospheric flanks and that nonlinear effects are unlikely to be significant for these modes on the flanks of the magnetosphere.

Fast body modes may couple to and drive FLRs in the magnetosphere [*Mills and Wright*, 1999]. However, these globally oscillatory modes have proved surprisingly elusive in data, suggesting that the body of the flanks of the magnetosphere are not significantly disrupted. The large e-folding lengths of these modes explains why they would be hard to observe. However, they may still drive FLRs as they convect around the magnetosphere. If the fast body modes are driven impulsively, the FLRs will be driven for a finite number of cycles as the modes convect past. If the modes are continuously driven, the FLRs will also be continuously driven, but the amplitude of the driving modes (the fast modes) will remain small. In either case the fact that the modes are convectively unstable helps to explain why the linear theory of FLRs has been so successful. Figure 16 gives a summary of these results with a schematic diagram showing the regions of the magnetosphere we are considering.

We have also studied the stability of the KH surface and body slow mode wavepackets which may only propagate at oblique angles to the flow, which are all convectively unstable in the magnetospheric rest frame. We found that slow surface modes will have e-folding lengths of the order of 100 R_E, and slow body modes will e-fold over distances of upward of 1000 R_E. Thus these modes will not grow to any significant amplitude as they convect over the flanks of the magnetosphere.

We have compared our results to those from a two-dimensional, time-dependent MHD code and found that the asymptotic behavior predicted by our method agrees well with that found in the code at large times. We have seen how the modes convect past a fixed point in the magnetosphere leaving zero displacement at large time. We have also seen that for an equilibrium with more than one unstable normal mode, the initial wavepacket may split into two parts corresponding to the different normal modes. In the reference frame of our simulation both these wavepackets are absolutely unstable and so will ultimately perturb every point in space. Thus these wavepackets will not totally split, but their centers will be seen to move apart.

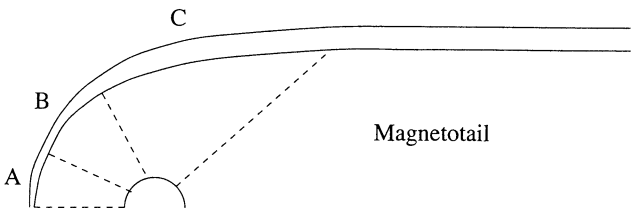

Figure 16. A schematic of the regions of the magnetosphere we are considering.

In the preliminary study we have presented here the magnetic field in the magnetosheath and low-latitude boundary layer (LLBL) has been neglected. Such an omission is not important for the antisunward propagating modes we consider here if the background field were to be directed northward. This is because the waves do not bend the field lines and so the stabilizing effect of field line tension is absent. Indeed, just such an equilibrium field is often adopted in modeling [e.g., *Miura*, 1984; *Wu*, 1986] because it is simple and represents the most unstable configuration in which the physics can be most easily studied. Moreover, satellite data confirm that at times it is a realistic configuration [*Manuel and Samson*, 1993].

Allowing the magnetosheath and LLBL field to have a more general orientation normally introduces some stabilization, and this has been addressed by *Miura* [1995a]. The stabilizing effect of the field need not dramatically alter the conclusions of our work. For example, *Manuel and Samson* [1993] considered the e-folding length of the convective instability: They compared the case in which the sheath and LLBL field was directed northward (no field line tension stabilization) and that in which the field was tilted through 30°. The latter case was more stable, and consequently they grew over a larger e-folding length that was 5% greater than the former. Hence the qualitative behavior of the two configurations is the same. It is interesting to note that the Parker spiral is tangential to the dusk flank but not to the dawn flank. *Mann and Wright* [1999] have suggested there should be a statistical bias for the Kelvin-Helmholtz instability to operate more often on the dawn flank, and this may account for the common azimuthal phase speeds of field line resonances which occur preferentially on that flank.

7. Summary

The interpretation of our results for strong solar wind flow are shown in Figure 16 and Table 1. This figure builds on a similar diagram of *Mann and Wright* [1999], which identified regions where waveguide modes would be leaky, stable, or unstable. Our calculations can provide a more detailed picture of the growth and propagation of the modes.

In region A, there is a small change in equilibrium flow speed, the LLBL is narrow, and surface mode wavepackets will be absolutely unstable. Waveguide modes will leak energy through the magnetopause here.

Table 1. Summary of the Properties of Fast-Mode Wavepackets in the Regions Shown in Figure 1b

Region	Δv, km/s	LLBL Width/R_E	Fast Surface Modes	Waveguide Modes
A	$\Delta v < 100$	<0.5	absolutely unstable	leaky
B	$100 < \Delta v < 400$	0.5→1.5	convectively unstable $L_e \sim 2R_E$ nonlinear effects → LLBL	trapped
C	$\Delta v > 400$	~1.5	convectively unstable $L_e \sim 7R_E$	convectively unstable $L_e \sim 20R_E$ driving of FLRs

In region B the increased change in flow speed provides perfect trapping for waveguide modes, while the surface mode wavepacket has now become convectively unstable with an e-folding length of the order of an Earth radius (in the rest frame of the Earth). These surface mode disturbances will quickly become nonlinear, and *Manuel and Samson* [1993] suggest that this can account for the broadening of the LLBL away from noon.

For slow solar wind conditions, region B may extend all the way to the near-Earth tail. However, for strong solar wind flow we expect a region C on the flanks, with a broad LLBL. The equilibrium here can support convectively unstable surface mode wavepackets (with e-folding lengths of $\sim 7\ R_E$ and convectively unstable waveguide mode wavepackets (with e-folding lengths of $\approx 20\ R_E$. The waveguide modes will only grow by a factor of about e as the convect tailward, and so should remain linear. They can also couple to field line resonances (FLRs).

Figure 17 shows a schematic summary for the dawn flank. The convectively unstable surface mode wavepacket has become nonlinear and broadened the LLBL. Two wavepackets are shown propagating tailward, and are associated with the first two convectively unstable waveguide mode wavepackets. Each of these wavepackets excites an FLR which it leaves in its wake, standing on closed field lines. The waveguide modes will have different tailward group velocities, but the wavepackets are likely to overlap as are the local times of the FLRs they excite. Such FLRs would be expected to have a common tailward phase speed [*Mills and Wright*, 1999], and this is a useful clue as the the mechanism through which the waveguide modes are excited.

Appendix A: The Theory of Absolute and Convective Instabilities

The space-time response of a plasma $\psi(y,t)$ is defined by the Laplace-Fourier integral

$$\psi(y,t) = \int_{-\infty+i\sigma}^{\infty+i\sigma} \int_{-\infty}^{\infty} \frac{w(\omega,k_y)}{D(\omega,k_y)} e^{i(k_y y-\omega t)} dk_y d\omega, \tag{A1}$$

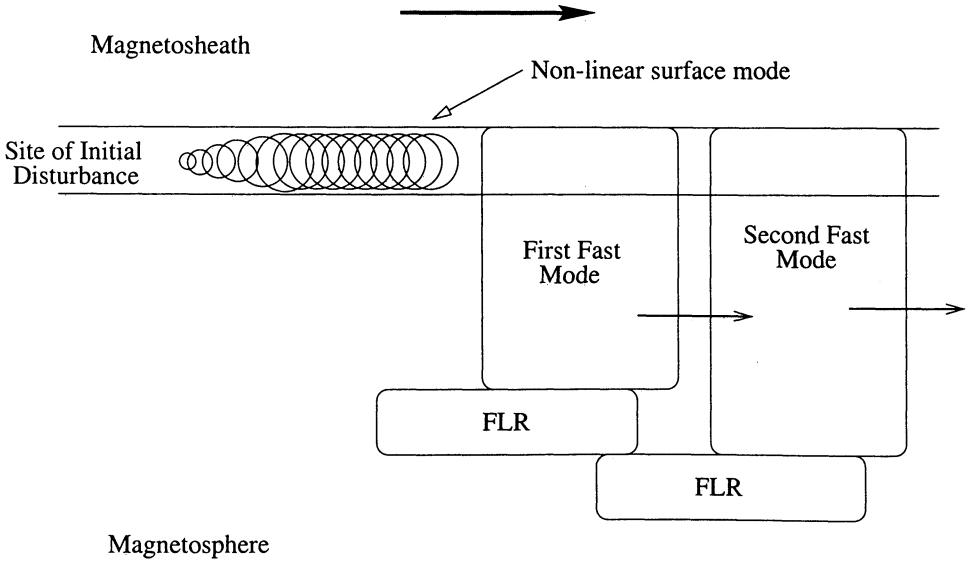

Figure 17. A schematic of the overall effect of disturbances on the magnetospheric flanks.

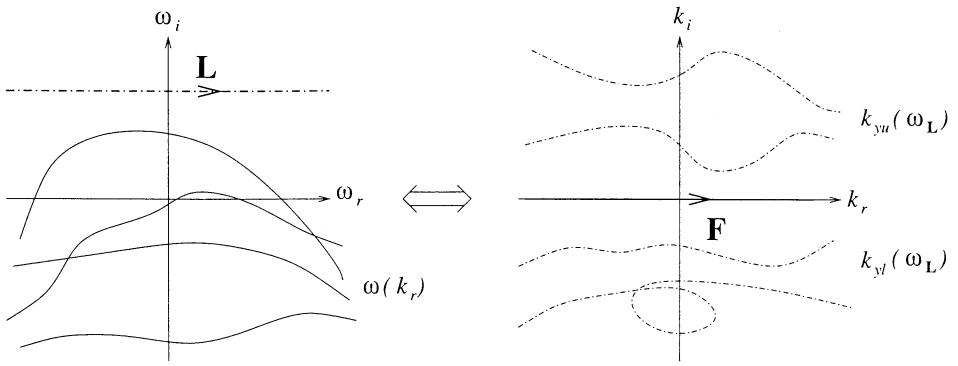

Figure 18. The mappings through the dispersion relation $D(\omega, k_y) = 0$ from the Laplace contour, L, onto the complex k_y plane showing the division of roots into k_{yu} (upper k_y plane) and k_{yl} (lower k_y plane). Also shown is the mapping from the Fourier contour F onto the complex ω plane, showing that all the roots occur below the Laplace contour.

where σ is defined to be larger than the largest growth rate of any mode for real k_y. The line along which we integrate in the complex ω plane is know as the Laplace or Bromwich contour. In the k_y plane we describe our integration path as the Fourier contour. In general, we may consider modes propagating at oblique angles to the flow, so that there is a finite wavenumber in the z direction. The component k_z enters the dispersion relation as a fixed parameter, and so we do not indicate it explicitly in the dispersion relation. Moreover, since each k_z mode decouples from the others, we may consider each one individually and sum over the permitted values subsequently. Since the most unstable flank modes will have $k_z = 0$, the majority of this paper focuses on these modes.

We may map the Laplace contour onto the complex k_y plane through the dispersion relation, and we find that each branch of the solution must lie either wholly in the upper half of the k_y plane (having $k_{yi} > 0$ and denoted k_{yu}) or the lower half of the plane (having $k_{yi} < 0$ and denoted k_{yl}). This follows from the fact that there are no solutions of the dispersion relation for real k_y for which $\omega_i = \sigma$ since σ is (by definition) greater than $\mathrm{Im}\{\omega(k_{yr})\}$. Similarly, the Fourier contour may be mapped onto the complex ω plane, and all the branches of this solution must lie below the Laplace contour. The positions of the two contours and the mappings between the two planes is shown in Figure 18.

In order to determine the asymptotic time response of the plasma we attempt to lower the Laplace contour. If the whole of the Laplace contour may be placed below the real ω axis, the instability is convective. Otherwise, it is absolute. Thus we take one point on the Laplace contour, say ω_{L1}, and keeping the same value of ω_r reduce the value of ω_i. We map the roots of the dispersion relation corresponding to ω_{L1} onto the k plane and follow their movement as we change ω_i as shown in Figure 19. Some of the roots in the k_y plane may cross the real k_y axis, however, so long as the Fourier contour may be deformed to remain above all the k_{yl} roots and below the k_{yu} roots, we may continue to reduce ω_i. However, if one k_{yu} root and one k_{yl} root move to the same point as we reduce ω_i (as seen in Figure 19) we can no longer deform the Fourier contour between these two points and therefore can no longer lower the Laplace contour at this value of ω_r. The point where two roots meet is

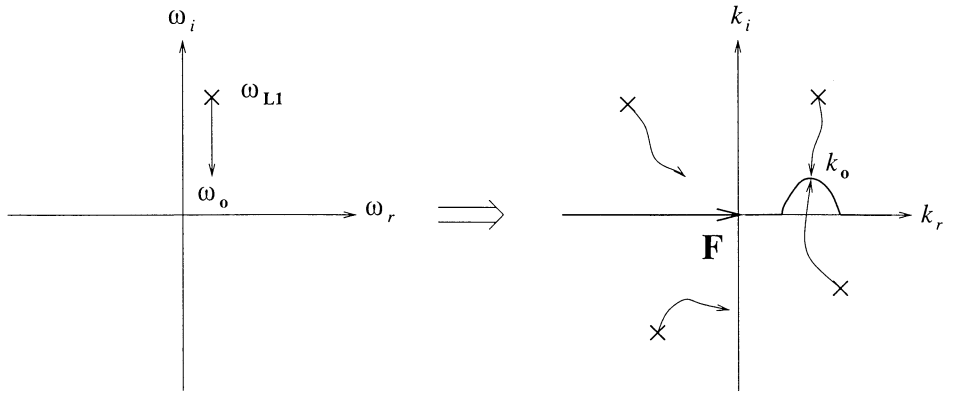

Figure 19. The mapping of the roots of the dispersion relation $D(\omega, k) = 0$ onto the complex k_y plane as ω_i is reduced from its value on the Laplace contour. Here two roots merge forming a "pinching" double root, which inhibits the further reduction of ω_i for this value of ω_r.

a double root of the dispersion relation, which satisfies (1). The double root of the dispersion relation must result from the merging of one k_{yu} root and one k_{yl} root, otherwise the Fourier contour may continue to be deformed between the two sets of roots. This condition is called the "pinching" condition. The asymptotic time response of the plasma is then defined by (2), using the "pinching" double root with the largest imaginary part of ω.

Double roots of the dispersion relation in the magnetospheric rest frame must also be saddle points of $\omega\,(k_y)$, and we can use this fact to identify a double root with each normal mode of the system for real k_y. In a reference frame moving with a speed v_f, $\omega' = \omega - k_y v_f$ must have a saddle point at a double root. We demand that the double root must be on the real k_y axis and take the derivative of ω' with respect to k_y. We obtain

$$\frac{\partial \omega'}{\partial k_y} = \frac{\partial \omega}{\partial k_y} - v_f = \frac{\partial \omega_r}{\partial k_y} - v_f + i\frac{\partial \omega_i}{\partial k_y}, \qquad \text{(A2)}$$

which must be zero at a saddle point. Therefore we require that $\partial\omega_i/\partial k_y = 0$ (i.e., we are at a maximum of the growth rate for real k_y) and

$$\frac{\partial \omega_r}{\partial k_y} = v_f, \qquad \text{(A3)}$$

so that we must be in a reference frame moving with the group velocity of the fastest growing normal mode. Thus we have identified a double root of the dispersion relation in the reference frame moving with this speed. We now follow the double root as we change reference frames to determine the absolute or convective nature of the instability as a function of reference frame.

Acknowledgments. K.J.M. is supported by a U.K. PPARC Research Studentship, A.N.W. is supported through a U.K. PPARC Advanced Fellowship, and A.W.L. and M.S.R. are supported by U.K. PPARC post-doctoral positions.

Janet G. Luhmann thanks Shigeru Fujita and Zuyin Pu for their assistance in evaluating this paper.

References

Bers, A., Space-time evolution of plasma instabilities - Absolute and convective, in *Handbook of Plasma Physics I,*, vol. 1, *Basic Plasma Physics I*, edited by M. N. Rosenbluth and R. Z. Sagdeev, p. 1, North-Holland, New York, 1983.

Brevdo, L., Absolute and convective instabilities and the e^N method for the prediction of the laminar-turbulent transition, *Z. Angew. Math. Mech., 74,* T340, 1994.

Briggs, R. J., *Electron-Stream Interaction With Plasmas, Res. Monogr.* no. 29, M.I.T Press, Cambridge, Mass., 1964.

Dungey, J. W., Electrodynamics of the outer atmosphere, *Sci. Rep. 69,* Pa. State Univ., Univ. Park, State College, 1954.

Fejer, J. A., Hydromagnetic stability at a fluid discontinuity between compressible fluids, *J. Fluid Mech., 7,* 499, 1964.

Fujita, S., K.-H. Glassmeier, and K. Kamide, MHD waves generated by the Kelvin-Helmholtz instability in a nonuniform magnetosphere, *J. Geophys. Res., 101,* 27, 317, 1996.

Landau, L. D., and E. M. Lifshitz, *Electrodynamics of continuous media,* (in Russian), p. 141, G.I.T.T.L., Moscow, 1953.

Mann, I. R., and A. N. Wright, Diagnosing the excitation mechanisms of Pc5 magnetospheric flank waveguide modes and FLRs, *Geophys. Res. Lett.* in press, 1999.

Mann, I. R., A. N. Wright, K. J. Mills, and V. M. Nakariakov, Excitation of magnetospheric waveguide modes by the magnetosheath flow, *J. Geophys. Res., 104,* 333, 1999.

Manuel, J. R., and J. C. Samson, The spatial development of the low latitude boundary layer, *J. Geophys. Res., 98,* 17,367, 1993.

Mills, K. J., and A. N. Wright, Azimuthal phase speeds of field line resonances driven by Kelvin-Helmholtz unstable waveguide modes, *J. Geophys. Res., 104,* 22,667, 1999.

Mills, K. J., A. N. Wright, and I. R. Mann, Kelvin-Helmholtz driven modes of the magnetosphere, *Phys. of Plasmas, 6: (10),* 4070, 1999.

Miura, A., Anomalous transport by magnetohydrodynamic Kelvin-Helmholtz instabilities in the solar wind-magnetosphere interaction, *J. Geophys. Res., 89,* 801, 1984.

Miura, A., Simulation of Kelvin-Helmholtz instability at the magnetosphere boundary, *J. Geophys. Res., 92,* 3195, 1987.

Miura, A., Dependence of the magnetopause Kelvin-Helmholtz instability on the orientation of the magnetosheath magnetic field, *Geophys. Res. Lett., 22,* 2993, 1995a.

Miura, A., Kelvin-Helmholtz instability at the magnetopause: Computer simulations, in *Physics of the Magnetopause, Geophysical Monograph Ser.*, vol. 90, edited by P. Song, B. U. O. Sonnerup, and M. F. Thomsen, p. 285, AGU, Washington, D. C., 1995b.

Pu, Z. Y., and M. G. Kivelson, Kelvin-Helmholtz instability at the magnetopause: Solution for compressible plasmas, *J. Geophys. Res., 88,* 841, 1983.

Ruderman, M., and A. N. Wright, Excitation of resonant Alfvén waves in the magnetosphere by negative energy surface waves on the magnetopause, *J. Geophys. Res., 103,* 26, 573, 1998.

Sen, A. K., Effect of compressibility on Kelvin-Helmholtz instability in a plasma, *Phys. Fluids, 7,* 1293, 1964.

Southwood, D. J., The hydromagnetic stability of the magnetospheric boundary, *Planet. Space Sci., 16,* 587, 1968.

Twiss, R. Q., On oscillations in electron streams, *Proc. Roy. Soc. London, Ser. B, 64,* 654, 1951.

Twiss, R. Q., Propagation in electron-ion streams, *Phys. Rev., 88,* 1392, 1952.

Walker, A. D. M., The Kelvin-Helmholtz instability in the low-latitude boundary layer, *Planet. Space Sci., 29,* 293, 1981.

Wright, A. N., K. J. Mills, M. S. Ruderman, L. Brevdo, The absolute and convective instability of the magnetospheric flanks, *J. Geophys. Res., 105,* 385, 2000.

Wu, C. C., Kelvin-Helmholtz instability at the magnetopause boundary, *J. Geophys. Res., 91,* 3042, 1986.

A. W. Longbottom, K. J. Mills, M. S. Rudermann, and A. N. Wright, Department of Mathematical and Computational Sciences, University of St. Andrews, Fife KY16 9SS, UK. (aaron@mcs.st-and.ac.uk, katie@mcs.st-and.ac.uk, michaelr@mcs.st-and.ac.uk, andy@mcs.st-and.ac.uk)

(Received August 12, 1999; revised March 21, 2000; accepted April 3, 2000.)